Articles in PresS. J Neurophysiol (August 6, 2014). doi:10.1152/jn.00320.2014

Subtype-Dependent Postnatal Development of Direction- and Orientation-Selective Retinal Ganglion Cells in Mice

Hui Chen[1], Xiaorong Liu[1, 2*], Ning Tian[3*]

1. Department of Ophthalmology, 2. Department of Neurobiology, Northwestern University, Evanston, Illinois 60208; 3. Department of Ophthalmology and Visual Science, University of Utah, Salt Lake City, Utah 84132

*: Corresponding authors:

Xiaorong Liu: xiaorong-liu@northwestern.edu; 847-467-0529; Hogan 2-160, 2205 Tech Drive, Northwestern University, Evanston, IL, 60208;

Ning Tian: Ning.Tian@hsc.utah.edu; 801-213-2852; Bldg. 523, S5160 JMEC, 65 Mario Capecchi Drive, John A. Moran Eye Center, Salt Lake City, Utah 84132

Running Title: Development of DSGCs and OSGCs

Copyright © 2014 by the American Physiological Society.

ABSTRACT

The direction-selective ganglion cells (DSGCs) and orientation-selective ganglion cells (OSGCs) encode the directional and the orientational information of a moving object, respectively. It is unclear how DSGCs and OSGCs mature in the mouse retina during postnatal development. Here we investigated the development of DSGCs and OSGCs after eye-opening. We show that (1) DSGCs and OSGCs are present at postnatal day 12 (P12), just before eye-opening; (2) the fractions of both DSGCs and OSGCs increase from P12 to P30; (3) the development of DSGCs and OSGCs are subtype-dependent; and (4) direction- and orientation- selectivity are two separate features of retinal ganglion cells (RGCs) in the mouse retina. We classified RGCs into different functional subtypes based on their light response properties. Compared to P12, the direction- and orientation- selectivity of ON-OFF RGCs but not ON RGCs became stronger at P30. The tuning width of DSGCs for both ON and ON-OFF subtypes decreased with age. For OSGCs, we divided them into non-DS OSGCs and DS&OSGCs. For DS&OSGCs, we found that there was no correlation between the direction- and orientation- selectivity and that the tuning width of both ON and ON-OFF subtypes remained unchanged with age. For non-DS OSGCs, the tuning width of ON but not ON-OFF subtype decreased with development. These findings provide a foundation to reveal the molecular and synaptic mechanisms underlying the development of the direction- and orientation- selectivity in the retina.

KEYWORDS: Retinal Ganglion Cell (RGC), Multi-electrode Array (MEA), Direction Selective Ganglion Cell (DSGC), Orientation Selective Ganglion Cell (OSGC).

INTRODUCTION

Different types of RGCs are tuned to respond to different features of visual scenes. For example, DSGCs extract motion information from the visual field i.e. they respond maximally when a stimulus moves in one direction (preferred) but little or no response when the stimulus moves in the opposite direction (null) (Barlow and Hill 1963; Oyster and Barlow 1967). By contrast, OSGCs (also called "axis-selective" RGCs) detect local bars and edges in the visual field and encode their orientations (Levick 1967). In other words, OSGCs selectively respond to the alignment orientation of stimuli as opposed to the direction of its movement.

The response properties of individual DSGCs have been characterized in rabbits (Fried et al. 2002; He and Masland 1997; Lee et al. 2010), and OSGCs in primates (Passaglia et al. 2002), cats (Levick and Thibos 1982), rabbits (Bloomfield 1994; He et al. 1998; Venkataramani and Taylor 2010), and mice (Zhao et al. 2013). Because mouse genetics in particular allows for the examination of functions and circuitry of defined cell types, studies in mice have started to reveal the synaptic mechanisms underlying the direction selectivity of RGCs (Briggman et al. 2011; Wei et al. 2011). It is still not clear whether and how the physiological properties of DSGCs and OSGCs mature during postnatal development. Previous studies reported that DSGCs are present around the time of eye opening in rabbits (Chan and Chiao 2008) and mice (Chen et al. 2009; Elstrott et al. 2008), suggesting that visual experience and patterned activity were not required to produce direction selectivity. However, the directional preference of DSGCs can be altered by adaptive moving stimulation (Rivlin-Etzion et al. 2012), indicating a possible activity-dependent plasticity for DSGCs. In addition, the tuning width of ON-OFF

DSGCs decreased and the distribution of the preferred directions became more symmetric after eye opening (Elstrott et al. 2008), suggesting that some properties of DSGCs continue to mature with age. At the same time, little is known of the development of OSGCs in the mouse retina, especially whether the development of orientation-selectivity correlates with the development of direction- selectivity. In this paper, we examined the developmental changes of the populations of DSGCs and OSGCs in the mouse retina.

METHODS

Animals. C57BL/6 wild type (WT) mice of either sex reared in 12h light/12h darkness were used in this study. All animal procedures conformed to the guidelines on the Use of Animals in Neuroscience Research from the NIH and were approved by the Institutional Animal Care and Use Committee at Yale University and University of Utah.

Multi-Electrode Array (MEA) recordings. Mouse retinas were dissected and then recorded using a 60-channel multielectrode array (MEA1060, Multichannel Systems Gmbh, Reutlingen, Germany) (Cantrell et al. 2010; Feng et al. 2013; Tian and Copenhagen 2003; Zhao et al. 2013). Visual stimuli were generated by the VersionWorks (Vision Research Graphics, Inc. Durham, NH). The full-field flash stimulus consisted of 2 seconds of light ON followed by 8 seconds of light OFF repeating 50 times. Moving bar stimulus was used to evaluate the direction and orientation selectivity of RGCs. The moving bar was a white rectangle moving on a black background (600 μm × 4000 μm, 1000 μm/s at 30° intervals) repeating 50 times with pseudorandom sequences of 12 directions. The light-evoked action potentials were recorded, and the electrical signals were filtered between 100 Hz and 3 kHz and sampled at 25 kHz.

Spike waveforms recorded by each electrode were sorted into single units in Offline Sorter (PlexonInc, Dallas, TX) (Koehler et al. 2011; Nirenberg et al. 2001; Tian and Copenhagen 2003). Briefly, a threshold of 68 μV was used to detect action potentials, the first and second principal components (PC1 and PC2) calculated, and clusters formed with action potentials having similar principal components (Elstrott et al.

2008; Tian and Copenhagen 2003). We selected clusters that could be clearly isolated from other spread-out activities for further analysis. From each isolated cluster, we defined a template by selecting a small fraction of spikes (approximately 10-20% of the cluster) located in the center of the cluster. We also adjusted the value of fit tolerance manually in order to avoid overlaps among different clusters. Using this template and fit tolerance, we sorted the action potentials from individual clusters (Tian and Copenhagen 2003). For each sorted unit, an autocorrelation function was applied in order to eliminate potential contaminations from other cells or noise (Elstrott et al. 2008; Nirenberg et al. 2001). Because neurons have a refractory period of approximately 1 millisecond (ms), spikes in the first 1-ms bin of the autocorrelogram may represent electronic noise or spikes from other cells (Nirenberg et al. 2001). Our data showed that 95% of total units contained less than 2% of spikes within this 1-ms window (median of distribution: 0.3; data not shown). Because these spikes were known to be contaminants, they were removed from further analysis. In addition, we manually removed spikes with irregular waveforms, which were generally created by overlapping of two or more spikes in a short time period. Each step of the offline-sorting processes was cross-examined and confirmed by another independent observer. Finally, the timestamps of spikes from each unit were exported to MATLAB (Mathworks, Natick, MA), where custom analyses were applied.

The Response Dominance Index (RDI). Peristimulus time histograms (PSTHs) of individual units with a 10 ms bin width were generated from cells' responses to both full field-flash and moving bars. The RDI was determined with the scalar value:

$$RDI = \frac{R_{ON} - R_{OFF}}{R_{ON} + R_{OFF}}$$

where R_{ON} and R_{OFF} were the maximum ON and OFF responses, respectively (Cantrell et al. 2010; Tian and Copenhagen 2003). For full field flash stimuli, the R_{ON} and R_{OFF} were defined as the peak frequency during first half second of ON and OFF portions of the stimulus. For moving bar stimuli, the ON and OFF responses represented the responses when the bar moving into and out of the cell's receptive field (RF). For each direction, the ON and OFF responses were first determined as the clusters in the PSTHs, and then the peak frequencies were calculated from the ON and OFF clusters. The R_{ON} and/or R_{OFF} were defined as the maximum value of the peak frequencies from the 12 directions for each cell.

For both stimuli, the value of the RDI ranges from -1 to 1. We classified cells into three functional subgroups: cells with RDI smaller than -0.6 were defined as OFF dominating RGCs; cells with the RDI larger than 0.6 as ON dominating RGCs; and cells with the RDI between -0.6 and 0.6 as ON-OFF RGCs (Cantrell et al. 2010). Cells that exhibited different response properties (< 10% of all cells recorded) were analyzed manually if the cell had clear clusters of ON and/or OFF responses in the PSTHs to the moving bar.

Direction Selectivity Index (DSI) and Orientation Selectivity Index (OSI).

DSI was calculated as:

$$DSI = \frac{R_{pref} - R_{null}}{R_{pref} + R_{null}}$$

where R_{pref} was the peak response at the preferred direction, defined as the stimulus direction with the maximum response, and R_{null} was the peak response at the opposite

direction. Cells with a DSI near 1 had response only at the preferred direction but no response at null direction, and cells with a DSI near 0 had responses with same strength at both preferred and null directions. For ON-OFF RGCs, the maximum value of DSI either from ON or OFF responses was selected as the DSI for the cell.

Most studies had used DSI cutoff of 0.33 i.e. when the R_{pref} was 2-folds larger than the R_{null}, the cell was classified as a DSGC (Rivlin-Etzion et al. 2012; Sun et al. 2011; Zhao et al. 2013); but see (Rivlin-Etzion et al. 2011), which used DSI cut-off value of 0.4 and (Elstrott et al. 2008) used 0.6. In this study, we mainly used 0.33 as the DSI cut-off and also tested other cutoff values.

OSI was defined as:

$$OSI = \frac{R_{pref} - R_{orth}}{R_{pref} + R_{orth}}$$

where R_{pref} was the peak response at the preferred orientation, and R_{orth} was the mean response at the two directions orthogonal to the preferred one. Similarly to DSGCs, cells with an OSI near 1 have response only at preferred orientation, and cells with an OSI near 0 have responses with same strength at both preferred and orthogonal orientations. We again used 0.33 as the cutoff to separate cells into OSGCs and non-OSGCs.

The responses at 12 directions were fitted with a bimodal Gaussian, as follows:

$$R = R_0 + A_1 \times e^{\frac{\cos(\theta - \theta_{pref}) - 1}{\sigma^2}} + A_2 \times e^{\frac{\cos(\theta - \theta_{pref} - \pi) - 1}{\sigma^2}}$$

where R is the response, θ is the direction, R_0 is the baseline, θ_{pref} is the preferred direction, σ is the SD, and A_1 and A_2 are the peak amplitudes (Zhao et al. 2013). Fitted tuning curves with R^2 larger than 0.3 were used for further analysis. The peak of the fitted

curve around the preferred direction was selected and then the tuning width was defined as the full-width of the half-maximum of the peak.

A student *t*-test was used to examine the difference between paired samples and a Kolmogorov-Smirnov (K-S) test to compare the distributions of continuous-valued variables (such as the DSI and the OSI). A two sample χ^2 test was used to compare distributions of categorical variables (such as percentage ON, OFF, and ON-OFF RGCs). Data was expressed as the mean ± SEM (Standard Error of Mean). The R square value was calculated as a measure of the goodness-of-fit in linear regression. Statistical analyses and graphing were done in Prism (GraphPad Software Inc., La Jolla, CA).

RESULTS

Characterization of RGC direction selectivity using the moving bar stimuli.

Retinas were dissected and RGC responses to the moving bar stimuli were recorded at P12 (n = 615 cells) and P30 (n = 425 cells, Fig. 1A). The ON and/or OFF dominated responses of each cell were characterized by RDI (see Methods for details). We also confirmed a cell's ON and OFF responses using the full-filed flash stimulus (Fig. 1A) and found that around 90% of cells had the same ON and OFF responses to both the moving bar and the full-field flash stimuli (data not shown).

We compared the absolute value of RDIs for all cells recorded at P12 and P30. The mean absolute value of RDI was 1.5-fold higher at P30 (0.62 ± 0.02) than P12 (0.42 ± 0 .01; $p < 0.001$ in Student's *t*-test), indicating the maturational transition from ON-OFF to ON or OFF dominated RGCs. Because RGC response properties may vary from experiment to experiment (Chichilnisky and Kalmar 2002), we examined whether the age-dependent change of RDI was due to the recording variation in different experiments. We compared the RDIs of RGCs from individual retinas at P12 and P30 (n = 4 in each group, Fig. 1B). Although there were some variations within the same age group, the distribution of the RDIs from the two age groups has minimum overlap and the difference of the RDIs from the two groups was significant ($p < 0.001$ in ANOVA test, Fig. 1B). Our data suggest that the change of RDIs with age was not due to the variation of individual experiments.

We classified RGCs into ON, OFF, and ON-OFF three functional subgroups as described in Method. We confirmed that the percentage of ON RGCs increased from

19.5% at P12 to 41.2% at P30, and ON-OFF RGCs decreased from 69.6% at P12 to 47.8% at P30 ($p < 0.001$ in χ^2 test, Fig. 1C and Table 1). These results are consistent with our previous findings on the maturational transition from ON-OFF to ON or OFF RGCs after eye-opening (Cantrell et al. 2010; Tian and Copenhagen 2003).

We next determined whether the change of cell-type percentage was due to the change of a cell's light response strength with age. We calculated the mean peak firing rate to full field flash stimuli and found it increased from P12 (26.5 ± 0.8 spikes/sec, n = 615) to P30 (34.5 ± 1.5 spikes/sec, n = 425; $p < 0.001$ in Student's *t*-test). We next examined the correlations between the RDI and the peak firing rate at P12 and P30. As shown in Fig. 1D, there was no linear correlation between the absolute value of RDI and the peak firing rate ($R^2 = 0.01$ at P12 and $R^2 = 0.02$ at P30). Together our data suggest that the cell-type percentage was not affected by cells' light response strength.

The direction selectivity of RGCs enhanced with age.

We calculated the DSI for individual RGCs using the response magnitude at preferred and null directions (see Methods for details; Fig. 2A). Robust DS responses were detected at P12 (Fig. 2A), as shown in previous studies (Chen et al. 2009; Elstrott et al. 2008). At two weeks after eye-opening (P30), the distribution of DSI shifted to the right compared to P12 (Fig. 2A), indicating that more RGCs with strong direction selectivity were detected at P30. The mean DSI at P30 was 0.33 ± 0.01 (n = 425), which was significantly higher than the mean DSI at P12 (0.26 ± 0.01, n = 615; $p < 0.001$ in Student's *t*-test; Fig. 2A).

We classified RGCs into ON, OFF, and ON-OFF subtypes and calculated the mean DSI of each functional subtype of RGCs at P12 and P30. The mean DSI of ON-OFF RGCs increased from P12 (0.28 ± 0.01, n = 428) to P30 (0.42 ± 0.02, n = 203; $p < 0.001$ in Student's *t*-test and K-S test; Fig. 2B). In contrast, the mean DSI for ON RGCs were not changed from P12 (0.21 ± 0.01, n = 120) to P30 (0.24 ± 0.01, n = 175; $p > 0.05$ in Student's *t*-test and K-S test; Fig. 2C); so was the OFF RGCs (P12: 0.21 ± 0.01, n = 67; P30: 0.26 ± 0.03, n = 47; $p > 0.05$ in Student's *t*-test and K-S test; Fig. 2D). We also confirmed that the enhanced direction selectivity with age was not due to the increase of peak firing rate. We performed a linear regression between the DSI and the peak firing rate of P12 and P30 RGCs and found that there was no correlation between the DSI and the peak firing rate for all three subtype RGCs ($R^2 < 0.2$, Fig. 2E-G).

Fraction of DSGCs increases with age.

We classified RGCs into DSGCs and non-direction-selective ganglion cell (non-DSGCs) (Fig. 3A). When the DSI exceeds 0.33, the 2:1 ratio for the preferred over null direction responses, we classified the cell as a DSGC. When the DSI is smaller than 0.33, we classified it as a non-DSGC. We find more DSGCs at P30 (42.6%) compared to P12 (27.8%; $p < 0.001$ in χ^2 test; Fig. 3B and Table 1). We also used a stricter criterion with DSI ≥ 0.5, a 3:1 ratio for the preferred over null direction responses, and further confirmed that the percentage of DSGCs increased with age (8.9% at P12 to 22.4% at P30, $p < 0.001$ in χ^2 test).

DSGCs were also classified into ON, OFF, and ON-OFF three subtypes (Fig. 3A). The fractions of ON and ON-OFF DSGCs increased from P12 to P30 (ON: 3.6% to

10.4%; ON-OFF: 22.1% to 29.4%), while OFF DSGCs were not changed (2.1% vs. 2.8%, Fig. 3C and Table 1). We excluded the OFF DSGCs from further analysis because of the small sampling numbers.

The development of direction selectivity is subtype-dependent.

For ON-OFF DSGCs, the cumulative distribution of DSI at P30 shifted to the right compared to P12 (Fig. 3D, $p < 0.001$ in K-S test), and the mean DSI increased from 0.47 ± 0.01 at P12 ($n = 136$) to 0.56 ± 0.01 at P30 (Fig. 3D insert; $n = 125$; $p < 0.001$ in Student's *t*-test). These results indicated that ON-OFF RGCs exhibited stronger direction selectivity at P30 than P12. By contrast, the cumulative distribution of DSI and the mean DSI of ON DSGCs (Fig. 3E) showed no significant difference between P12 and P30 (P30: 0.51 ± 0.03, $n = 44$; P12: 0.48 ± 0.03, $n = 22$; $p = 0.85$ in K-S test, and $p = 0.46$ in Student's *t*-test).

The tuning widths of DSGCs were calculated at P12 and P30 (Fig. 3F-H). At P12, the mean tuning width for ON-OFF DSGCs was $82.0 \pm 3.8°$ ($n = 93$) and the ON DSGCs was $95.0 \pm 8.8°$ ($n = 17$). At P30, the mean tuning width decreased for both ON-OFF ($71.5 \pm 3.3°$, $n = 91$) and ON DSGCs ($71.8 \pm 5.5°$, $n = 31$; $p < 0.05$ in Student's *t*-test; Fig. 3G-H). Our results show that the fractions of both ON-OFF and ON DSGCs increased and their tuning widths decreased; and that the direction selectivity of ON-OFF but not ON DSGCs was enhanced with age.

Fraction of OSGCs increases with age.

We next examined the OSGCs at P12 and P30. The OSI for each individual cell was calculated (see Methods for details) and cells were classified into OSGCs (OSI ≥ 0.33) and non-OSGCs (OSI < 0.33, Fig. 4A-B). The percentage of OSGCs increased from 29.3% at P12 to 47.8% at P30 ($p < 0.001$ in χ^2 test; Fig. 4B and Table 1). We also applied the cut-off value of 0.5 and found similar increase (7.6% at P12 to 22.6% at P30, $p < 0.001$ in χ^2 test). This increase is due to the increase of the percentages of both ON and ON-OFF OSGCs (ON: 4.1% to 14.1%; ON-OFF: 22.3% to 29.2%, $p = 0.001$ in χ^2 test; Fig. 4C and Table 1).

Since some OSGCs also showed direction selectivity, the above increase might reflect the increase of DSGCs as well. We thus divided OSGCs into two subtypes based on their DSI value: DS&OSGCs (with both OSI and DSI ≥ 0.33) and non-DS OSGCs (DSI < 0.33 and OSI ≥ 0.33, Fig. 4A). In other words, DS&OSGCs exhibited the characteristic of both orientation- and direction- selectivity, and non-DS OSGCs exhibited strong orientation- but not direction- selectivity. We found that the fractions of both non-DS OSGCs and DS&OSGCs were increased from P12 to P30 (non-DS OSGCs: 15.8% to 19.5%; DS&OSGCs: 13.5% to 28.2%; Fig. 4D-E). Furthermore, the increase of non-DS OSGCs (Fig. 4D) was mainly due to the increase of ON cells (2.4% at P12 to 7.3% at P30). By contrast, the increase of DS&OSGCs (Fig. 4E) was due to the increases of both ON-OFF (11.4% at P12 to 20.2% at P30) and ON cells (1.6% at P12 to 6.8% at P30).

The development of OSGCs exhibits different patterns compared to the DSGCs.

The DS&OSGCs (with both OSI and DSI ≥ 0.33) have both strong direction- and orientation- selectivity, raising the possibility that the DS and OS properties might be regulated by the same mechanism in these cells. We thus examined the developmental profiles of the direction- and orientation- selectivity of DS&OSGCs. For ON-OFF cells, the mean DSI was 0.51 ± 0.02 (n = 55), and the mean OSI was 0.47 ± 0.02 (n = 55) at P12. They both increased with age (DSI at P30: 0.58 ± 0.02, n = 79, $p < 0.05$; OSI at P30: 0.55 ± 0.02, n = 79; $p < 0.01$ in Student's *t*-test and K-S test; Fig. 5A). In contrast, the mean DSI and mean OSI of the ON cells did not change significantly ($p > 0.05$ in Student's *t*-test and K-S test; Fig. 5B). The mean tuning widths of both ON-OFF and ON DS&OSGCs were similar between the two age groups (ON-OFF: 71.6 ± 4.1°, n = 53 at P12 and 64.2 ± 3.2°, n = 71 at P30; ON: 78.0 ± 7.6°, n = 10 at P12 and 66.7 ± 5.7°, n = 23 at P30; $p > 0.05$ in Student's *t*-test).

We next tested whether the direction selectivity correlated with the orientation selectivity for the DS&OSGCs. We performed a linear regression between DSI and OSI at P12 and P30. As shown in Figs. 5A and 5B (right panels), the correlation between DSI and OSI was very week ($R^2 < 0.2$). The slopes of the fitted lines at P12 and P30 were identical for both ON-OFF and ON DS&OSGCs. Together these results suggest that the direction- and orientation- selectivity are two distinct properties of RGCs.

We also examined whether the OSI of non-DS OSGCs (DSI < 0.33 and OSI ≥ 0.33) increased with age. For ON-OFF RGCs, the mean OSI of non-DS OSGCs was 0.51 ± 0.02 at P30 (n = 51), larger than that of P12 (0.41 ± 0.01, n = 84; $p < 0.001$ in Student's *t*-test and K-S test; Fig. 6A, left panel). Their tuning width exhibited no difference between P12 (57.7 ± 2.6°, n = 78) and P30 (60.2 ± 3.3°, n = 46; $p = 0.5$ in Student's *t*-test

and $p = 0.7$ in K-S test; Fig. 6A, right panel). By contrast, for ON RGCs, the mean OSI of non-DS OSGCs showed no significant change between P12 (0.45 ± 0.03, $n = 15$) and P30 (0.47 ± 0.03, $n = 31$; $p = 0.6$ in Student's *t*-test and $p = 0.7$ in K-S test; Fig. 6B, left panel). Their mean tuning width decreased from $70.3 \pm 6.0°$ at P12 ($n = 14$) to $49.8 \pm 3.6°$ at P30 ($n = 27$; $p < 0.01$ in Student's *t*-test and $p < 0.05$ in K-S test; Fig. 6B, right panel).

Taken together, our data showed that nearly one-third of RGCs were highly tuned for the direction or orientation of motion stimulus at the time of eye-opening. The percentages of DSGCs and OSGCs continued to increase with age. The direction- and orientation- selectivity was enhanced for ON-OFF but not ON RGCs with development. For DSGCs, the tuning width of both ON-OFF and ON subtypes decreased with age. For non-DS OSGCs, the tuning width decreased for ON but not ON-OFF subtype. Moreover, there was no correlation between the DSI and the OSI for DS&OSGCs. In other words, DSGCs and OSGCs mature differently in a subtype-dependent manner.

DISCUSSION

Classification of DSGCs

Three functional subgroups of DSGCs have been characterized: (1) ON DSGCs respond to global motion in one of three directions: upward, downward, or anterior (Oyster 1968; Oyster and Barlow 1967); (2) OFF DSGCs respond to upward motion (Kim et al. 2008); and (3) ON-OFF DSGCs respond preferentially to image motion in one of the four cardinal ocular directions: ventral, dorsal, temporal and nasal (Briggman et al. 2011; Elstrott et al. 2008; Oyster 1968; Oyster and Barlow 1967). In the rabbit retina, ON-OFF DSGCs account for about 21% of the total RGCs (Oyster 1968). In the mouse retina, different studies revealed quite a wide range of DSGCs. A recent study combined the two-photon calcium imaging with the serial-section electron microscopy and suggested about 10% DSGCs in the mouse retina (Briggman et al. 2011). One group of ON-OFF DSGCs labeled by DiI is counted for 16% of total RGCs (Sun et al. 2002), while another study suggested 21% (Xu and Tian 2007). Huberman and his colleagues (Huberman et al. 2009) suggested the total ON-OFF DSGCs is about 20 - 36%. Here we found about 29% of total RGCs are ON-OFF DSGCs (Fig. 3C and Table 1), which falls into the range in the above study. ON DSGCs are counted for 5% of the total RGCs in the rabbit retina (Oyster 1968) and 3 - 7% in the mouse retina (Sun et al. 2002; Xu and Tian 2007). Here we show ON DSGCs was ~10% at P30 (Fig. 3C and Table 1). The differences observed in these studies could be due to that (1) different visual stimulation was applied to identify DSGCs (see discussion below); and (2) different techniques may

have different sensitivity to detect certain population of RGCs; (3) RGC dendritic pattern and molecular markers may not completely correlate with its light response properties (Rivlin-Etzion et al. 2011, 2012).

Development of DSGCs and OSGCs

One study using drifting gratings showed that the distribution of the tuning width for ON-OFF DSGCs at P14 had a broader value range compared to the adult retinas (Elstrott et al. 2008). However, drifting gratings could generate adapted responses and even could reverse the directional preference (Rivlin-Etzion et al. 2012). Another study using the moving bar stimulus showed that the degree of direction selectivity of early postnatal DSGCs (both ON-OFF and ON DSGCs) was almost identical to that in adult retinas (Chen et al. 2009). When we applied the DSI cut-off value of 0.6 (a 4:1 ratio for the preferred over null direction responses) to identify DSGCs, we found that the mean DSIs and the tuning widths of DSGCs had no difference at P12 and P30 (data not shown). Our results are consistent with the notion that the fraction of highly direction-selective RGCs exist at the time of eye opening and exhibit similar directional turning properties as in adult retinas. However, when we used the DSI cut-off of 0.33 or 0.5 (a 2:1 or 3:1 ratio for the preferred over null direction responses), we find that both the fraction and the average DSI of DSGCs are higher at P30 than that at P12 (Fig. 3). These findings suggest that some DSGCs may continue to develop after eye-opening.

Recently it has been shown that OSGCs are abundant in the adult mouse retina (Zhao et al. 2013). Similarly to the DSGCs, both ON-OFF and ON OSGCs were detected

362 at P12, and the fraction of OSGCs increased from P12 to P30 (Fig. 4). However, OSGCs
363 exhibit different developing patterns compared to DSGCs (Fig. 5-6). Studies in the rabbit
364 retina found that orientation bias did not contribute to the generation of direction
365 selectivity (He et al. 1998). We also found no correlation between direction- and
366 orientation- selectivity in the mouse retina (Fig. 5). These findings support the notion that
367 direction- and orientation- selectivity are two distinct features of RGCs.

368 Different mechanisms for generating direction- and orientation- selectivity have
369 been suggested. The direction selectivity was generated by asymmetric inhibitory and
370 excitatory inputs and temporal offset between inhibitory and excitatory inputs (Vaney et
371 al. 2012; Wei and Feller 2011). Other studies suggest that an elongated RF could simply
372 contributed the orientation bias (Levick and Thibos 1982). Alternatively, orientation bias
373 could result from electrical coupling with neighboring RGCs of the same subtype (Volgyi
374 et al. 2009). The coupled cells may respond more to the orientation that cross their RFs.
375 Some studies also showed that the orientation selectivity is mediated by presynaptic
376 inhibition (Bloomfield 1994; Venkataramani and Taylor 2010). Much remain to be
377 investigated of the developmental mechanisms of DSGCs and especially OSGCs.
378

379 **Development of the Direction- and Orientation- Selectivity in the Visual System**

380 Orientation selectivity in cortical neurons was suggested to be built from un-tuned
381 thalamic inputs (Ferster and Miller 2000; Hubel and Wiesel 1962; Shapley et al. 2003;
382 Sompolinsky and Shapley 1997). However, recent studies in mice showed that the
383 orientation-selective cells are abundant in dorsal lateral geniculate nucleus (dLGN)
384 (Marshel et al. 2012; Piscopo et al. 2013; Scholl et al. 2013; Zhao et al. 2013), and the

orientation selectivity in dLGN does not require cortical feedback (Scholl et al. 2013; Zhao et al. 2013). These findings suggest that the orientation selectivity of some dLGN neurons might be transmitted from the retina (Zhao et al. 2013). In fact, there is a di-synaptic circuit linking DSGCs with the superficial layers of the primary visual cortex (V1), through a specialized subdivision of the dLGN (Cruz-Martin et al. 2014), further supporting the notion that the direction- and orientation- selectivity of some V1 neurons may be influenced by the activities of RGCs.

In addition, studies revealed some similarities between the development of direction- selectivity of the cortical neurons and the retinal neurons in mice (Elstrott et al. 2008; Rochefort et al. 2011). The direction selectivity of V1 neurons was first detected at the time of eye-opening and emerged independently of visual experience (Rochefort et al. 2011), similarly as in the retina (Elstrott et al. 2008). Furthermore, after eye-opening, the percentages of motion-sensitive and orientation-selective neurons in V1 increased (Rochefort et al. 2011), also similar as we observed in the retina. More work is needed to examine how the direction- and orientation- selectivity in the retina emerges and relays to the cortical neurons during postnatal development.

In summary, our data demonstrate that both DS and OS circuits continue to develop after eye opening in the mouse retina. The development of direction- and orientation- selectivity is subtype-dependent with different patterns. Our study provides the foundation to investigate the circuit functions that underlie the development of the direction- and orientation- selectivity in RGCs, and to understand the visual information processing in the visual system.

ACKNOWLEDGMENTS

We thank Drs. Jianhua Cang and John B. Troy, Mr. Brent K. Young and Mr. Kevin Huang for critical reading.

GRANTS

The work contained in this paper has been supported by the William & Mary Greve Special Scholar Award from the Research to Prevent Blindness (XL), Northwestern Memorial Foundation/Brinson Foundation (XL), the Illinois Society for the Prevention of Blindness (HC), and NIH grants R01EY012345 (NT), 5P30EY014800 (NT) and R01EY019034 (XL).

DISCLOSURES

No conflicts of interest, financial or otherwise, are declared by the author(s).

REFERENCES

Barlow HB, and Hill RM. Selective sensitivity to direction of movement in ganglion cells of the rabbit retina. *Science* 139: 412-414, 1963.

Bloomfield SA. Orientation-sensitive amacrine and ganglion cells in the rabbit retina. *J Neurophysiol* 71: 1672-1691, 1994.

Briggman KL, Helmstaedter M, and Denk W. Wiring specificity in the direction-selectivity circuit of the retina. *Nature* 471: 183-188, 2011.

Cantrell DR, Cang J, Troy JB, and Liu X. Non-centered spike-triggered covariance analysis reveals neurotrophin-3 as a developmental regulator of receptive field properties of ON-OFF retinal ganglion cells. *PLoS Comput Biol* 6: e1000967, 2010.

Chan YC, and Chiao CC. Effect of visual experience on the maturation of ON-OFF direction selective ganglion cells in the rabbit retina. *Vision Res* 48: 2466-2475, 2008.

Chen M, Weng S, Deng Q, Xu Z, and He S. Physiological properties of direction-selective ganglion cells in early postnatal and adult mouse retina. *J Physiol* 587: 819-828, 2009.

Chichilnisky EJ, and Kalmar RS. Functional asymmetries in ON and OFF ganglion cells of primate retina. *J Neurosci* 22: 2737-2747, 2002.

Cruz-Martin A, El-Danaf RN, Osakada F, Sriram B, Dhande OS, Nguyen PL, Callaway EM, Ghosh A, and Huberman AD. A dedicated circuit links direction-selective retinal ganglion cells to the primary visual cortex. *Nature* 507: 358-361, 2014.

Elstrott J, Anishchenko A, Greschner M, Sher A, Litke AM, Chichilnisky EJ, and Feller MB. Direction selectivity in the retina is established independent of visual experience and cholinergic retinal waves. *Neuron* 58: 499-506, 2008.

Feng L, Zhao Y, Yoshida M, Chen H, Yang JF, Kim TS, Cang J, Troy JB, and Liu X. Sustained ocular hypertension induces dendritic degeneration of mouse retinal ganglion cells that depends on cell type and location. *Invest Ophthalmol Vis Sci* 54: 1106-1117, 2013.

Ferster D, and Miller KD. Neural mechanisms of orientation selectivity in the visual cortex. *Annu Rev Neurosci* 23: 441-471, 2000.

Fried SI, Munch TA, and Werblin FS. Mechanisms and circuitry underlying directional selectivity in the retina. *Nature* 420: 411-414, 2002.

He S, Levick WR, and Vaney DI. Distinguishing direction selectivity from orientation selectivity in the rabbit retina. *Vis Neurosci* 15: 439-447, 1998.

He S, and Masland RH. Retinal direction selectivity after targeted laser ablation of starburst amacrine cells. *Nature* 389: 378-382, 1997.

Hubel DH, and Wiesel TN. Receptive fields, binocular interaction and functional architecture in the cat's visual cortex. *J Physiol* 160: 106-154, 1962.

Huberman AD, Wei W, Elstrott J, Stafford BK, Feller MB, and Barres BA. Genetic identification of an On-Off direction-selective retinal ganglion cell subtype reveals a layer-specific subcortical map of posterior motion. *Neuron* 62: 327-334, 2009.

Kim IJ, Zhang Y, Yamagata M, Meister M, and Sanes JR. Molecular identification of a retinal cell type that responds to upward motion. *Nature* 452: 478-482, 2008.

Koehler CL, Akimov NP, and Renteria RC. Receptive field center size decreases and firing properties mature in ON and OFF retinal ganglion cells after eye opening in the mouse. *J Neurophysiol* 106: 895-904, 2011.

Lee S, Kim K, and Zhou ZJ. Role of ACh-GABA cotransmission in detecting image motion and motion direction. *Neuron* 68: 1159-1172, 2010.

Levick WR. Receptive fields and trigger features of ganglion cells in the visual streak of the rabbits retina. *J Physiol* 188: 285-307, 1967.

Levick WR, and Thibos LN. Analysis of orientation bias in cat retina. *J Physiol* 329: 243-261, 1982.

Marshel JH, Kaye AP, Nauhaus I, and Callaway EM. Anterior-posterior direction opponency in the superficial mouse lateral geniculate nucleus. *Neuron* 76: 713-720, 2012.

Nirenberg S, Carcieri SM, Jacobs AL, and Latham PE. Retinal ganglion cells act largely as independent encoders. *Nature* 411: 698-701, 2001.

Oyster CW. The analysis of image motion by the rabbit retina. *J Physiol* 199: 613-635, 1968.

Oyster CW, and Barlow HB. Direction-selective units in rabbit retina: distribution of preferred directions. *Science* 155: 841-842, 1967.

Passaglia CL, Troy JB, Ruttiger L, and Lee BB. Orientation sensitivity of ganglion cells in primate retina. *Vision Res* 42: 683-694, 2002.

Piscopo DM, El-Danaf RN, Huberman AD, and Niell CM. Diverse visual features encoded in mouse lateral geniculate nucleus. *J Neurosci* 33: 4642-4656, 2013.

Rivlin-Etzion M, Wei W, and Feller MB. Visual stimulation reverses the directional preference of direction-selective retinal ganglion cells. *Neuron* 76: 518-525, 2012.

Rivlin-Etzion M, Zhou K, Wei W, Elstrott J, Nguyen PL, Barres BA, Huberman AD, and Feller MB. Transgenic mice reveal unexpected diversity of on-off direction-selective retinal ganglion cell subtypes and brain structures involved in motion processing. *J Neurosci* 31: 8760-8769, 2011.

Rochefort NL, Narushima M, Grienberger C, Marandi N, Hill DN, and Konnerth A. Development of direction selectivity in mouse cortical neurons. *Neuron* 71: 425-432, 2011.

Scholl B, Tan AY, Corey J, and Priebe NJ. Emergence of orientation selectivity in the Mammalian visual pathway. *J Neurosci* 33: 10616-10624, 2013.

Shapley R, Hawken M, and Ringach DL. Dynamics of orientation selectivity in the primary visual cortex and the importance of cortical inhibition. *Neuron* 38: 689-699, 2003.

Sompolinsky H, and Shapley R. New perspectives on the mechanisms for orientation selectivity. *Curr Opin Neurobiol* 7: 514-522, 1997.

Sun L, Han X, and He S. Direction-selective circuitry in rat retina develops independently of GABAergic, cholinergic and action potential activity. *PLoS One* 6: e19477, 2011.

Sun W, Li N, and He S. Large-scale morphological survey of mouse retinal ganglion cells. *J Comp Neurol* 451: 115-126, 2002.

Tian N, and Copenhagen DR. Visual stimulation is required for refinement of ON and OFF pathways in postnatal retina. *Neuron* 39: 85-96, 2003.

Vaney DI, Sivyer B, and Taylor WR. Direction selectivity in the retina: symmetry and asymmetry in structure and function. *Nat Rev Neurosci* 13: 194-208, 2012.

Venkataramani S, and Taylor WR. Orientation selectivity in rabbit retinal ganglion cells is mediated by presynaptic inhibition. *J Neurosci* 30: 15664-15676, 2010.

Volgyi B, Chheda S, and Bloomfield SA. Tracer coupling patterns of the ganglion cell subtypes in the mouse retina. *J Comp Neurol* 512: 664-687, 2009.

Wei W, and Feller MB. Organization and development of direction-selective circuits in the retina. *Trends Neurosci* 34: 638-645, 2011.

Wei W, Hamby AM, Zhou K, and Feller MB. Development of asymmetric inhibition underlying direction selectivity in the retina. *Nature* 469: 402-406, 2011.

Xu HP, and Tian N. Retinal ganglion cell dendrites undergo a visual activity-dependent redistribution after eye opening. *J Comp Neurol* 503: 244-259, 2007.

Zhao X, Chen H, Liu X, and Cang J. Orientation-selective Responses in the Mouse Lateral Geniculate Nucleus. *J Neurosci* 33: 12751-12763, 2013.

Figure Legends

Figure 1. Characterization of DSGCs by a 60-channel MEA system. **A**. RGCs were classified into ON, OFF and ON-OFF subtypes based on their responses to the moving bar (left) and/or full-field flash (right) stimuli. Left panel shows the white bar moving upon a black background. The circle illustrates a cell's receptive field (RF). Right panel shows the full screen flash stimuli (with MEA electrodes positioned at the center). **B.** The cumulative distribution of absolute values of RDI of all recorded RGCs of mice at P12 (n=4) and P30 (n=4). ON-OFF RGCs had RDI close to 0 while ON RGCs and OFF RGCs close to 1 or -1. Bin width: 0.05. **C.** More ON RGCs and fewer ON-OFF RGCs were found at P30 compared to P12 ($p < 0.001$ in χ^2 test). **D**. Plot of absolute RDI versus firing rate of RGCs at P12 and P30. Solid lines represent the linear regressions. The value of R^2 ranges from 0 to 1, with 0 representing no linear relationship and 1 perfect linear relationship between the two parameters.

Figure 2. The direction selectivity of RGCs enhanced with age. **A.** Top: Distributions of DSI from all RGCs at P12 and P30. Bottom: Representative recordings of RGCs with different DSIs. The tuning curve was calculated based on the peak spike frequency for 12 directions and plotted as a function of directions of the moving object (see Methods). **B-D**. Cumulative distributions of DSI from ON-OFF (B), ON (C) and OFF (D) RGCs at P12 and P30. Inserts: Mean DSIs of ON-OFF, ON and OFF RGCs at P12 and P30. **E-G**. Plots of DSI versus firing rate of ON-OFF (E), ON (F) and OFF (G) RGCs at P12 and

P30. Solid lines represent the linear regressions. *: $p < 0.05$; ***: $p < 0.001$; n.s.: not significant ($p > 0.05$) in K-S test and Student's *t*-test (same in Figures 3, 5 and 6).

Figure 3. Development of DSGCs is subtype-dependent. **A.** The schematic diagram of RGC classification. **B.** The percentage of DSGCs increased while non-DSGCs decreased from P12 to P30. $p < 0.001$ in χ^2 test. **C**. The percentages of both ON and ON-OFF DSGCs increased from P12 to P30. $p < 0.001$ in χ^2 test. **D-E.** Cumulative distributions of DSI for ON-OFF (D) and ON (E) DSGCs. Inserts: Mean DSIs of ON-OFF (D) and ON (E) DSGCs at P12 and P30. **F.** Tuning width was calculated as the full-width of the half-maximum of the fitted tuning curve (solid line, see Methods for details). **G-H.** The tuning width decreased with age for both ON-OFF (G) and ON (H) DSGCs. Inserts: Mean tuning width of ON-OFF and ON DSGCs at P12 and P30.

Figure 4. The fraction of OSGCs increases with age. **A.** The schematic diagram of RGC classification. **B.** The percentage of OSGCs increased while non-OSGCs decreased from P12 to P30. $p < 0.001$ in χ^2 test. **C**. The percentages of both ON and ON-OFF OSGCs increased from P12 to P30. $p < 0.001$ in χ^2 test. **D.** The increase of non-DS OSGCs was mainly due to the increase of ON cells. $p < 0.001$ in χ^2 test. **E.** The increase of DS&OSGCs was due to the increases of both ON-OFF and ON cells. $p < 0.001$ in χ^2 test.

Figure 5. For DS&OSGCs, the direction- and orientation- selectivity of ON-OFF cells were enhanced, while ON cells were unchanged. **A-B.** Left: Cumulative distributions of DSI for ON-OFF (A) and ON (B) DS&OSGCs at P12 and P30. Middle: Cumulative

distributions of OSI for ON-OFF and ON DS&OSGCs. Inserts: Mean OSIs and tuning widths of ON-OFF and ON DS&OSGCs. Right: Plots of DSI versus OSI of ON-OFF and ON DS&OSGCs show that their direction- and orientation- selectivity are not correlated. Solid lines represent the linear regressions.

Figure 6. Development of non-DS OSGCs is also subtype-dependent. **A-B.** Left: The OSI of ON-OFF (A) but not ON (B) non-DS OSGCs significantly increased from P12 to P30. Right: The tuning width of ON non-DS OSGCs decreased, while ON-OFF cells were unchanged. Inserts: Mean OSIs and tuning widths of ON-OFF and ON non-DS OSGCs.

Figure 1

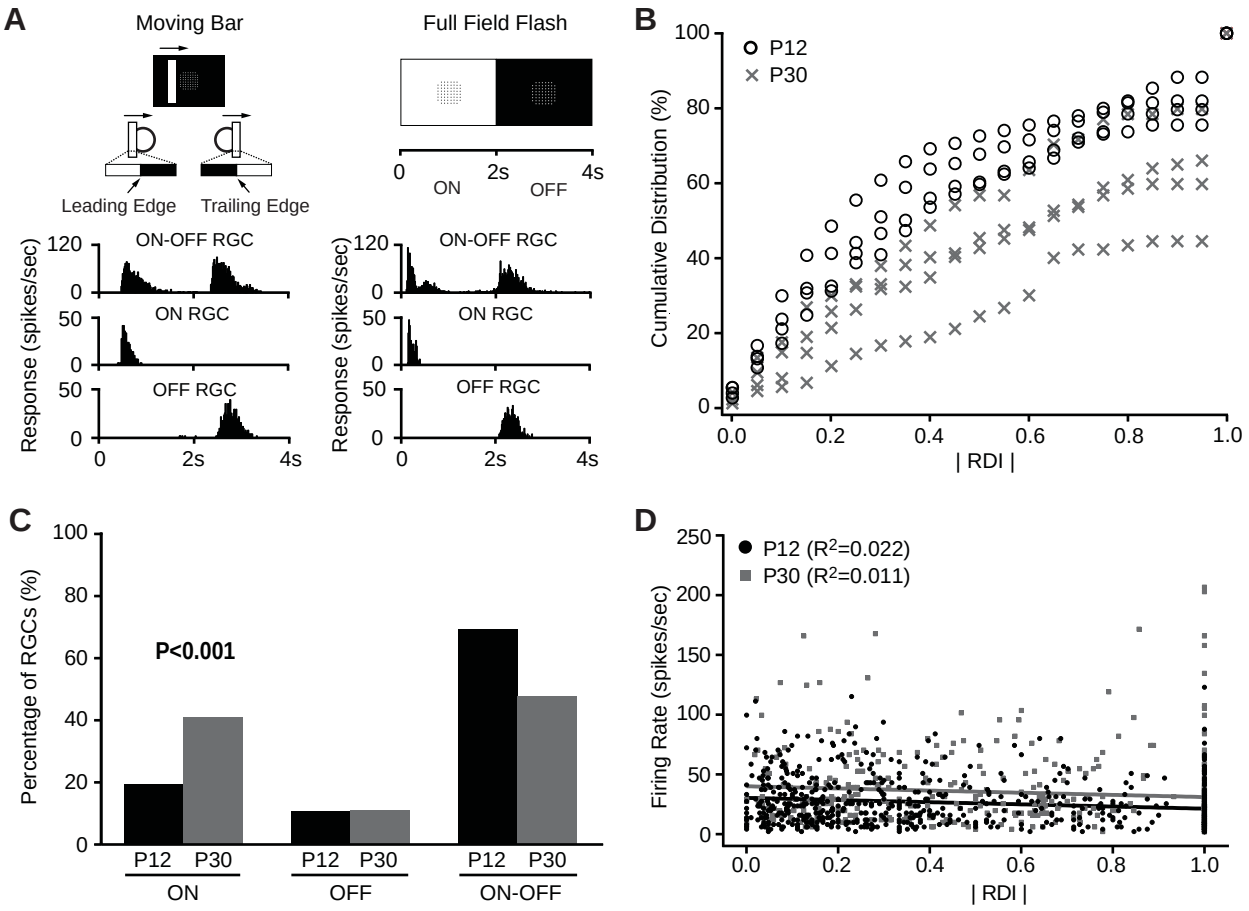
A
Moving Bar
Full Field Flash
Leading Edge
Trailing Edge
ON
OFF
ON-OFF RGC
ON RGC
OFF RGC
Response (spikes/sec)
B
P12
P30
Cumulative Distribution (%)
| RDI |
C
P<0.001
Percentage of RGCs (%)
P12 P30
ON
OFF
ON-OFF
D
P12 (R^2=0.022)
P30 (R^2=0.011)
Firing Rate (spikes/sec)
| RDI |

Figure 2

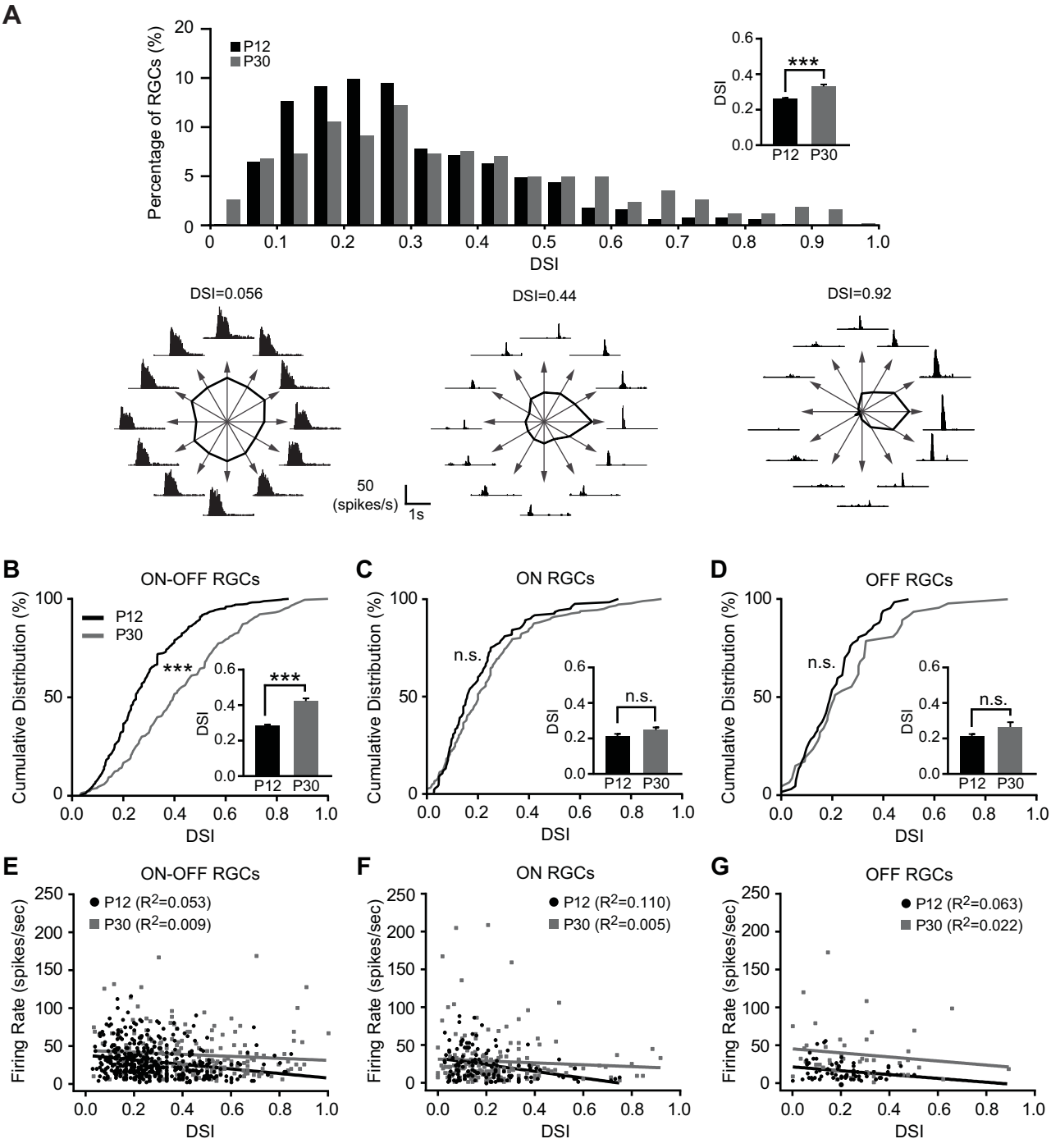
A
Percentage of RGCs (%)
P12
P30
DSI
***
DSI=0.056
DSI=0.44
DSI=0.92
50
(spikes/s)
1s
B
ON-OFF RGCs
Cumulative Distribution (%)
n.s.
C
ON RGCs
D
OFF RGCs
E
ON-OFF RGCs
Firing Rate (spikes/sec)
P12 (R^2=0.053)
P30 (R^2=0.009)
F
ON RGCs
P12 (R^2=0.110)
P30 (R^2=0.005)
G
OFF RGCs
P12 (R^2=0.063)
P30 (R^2=0.022)

Figure 3

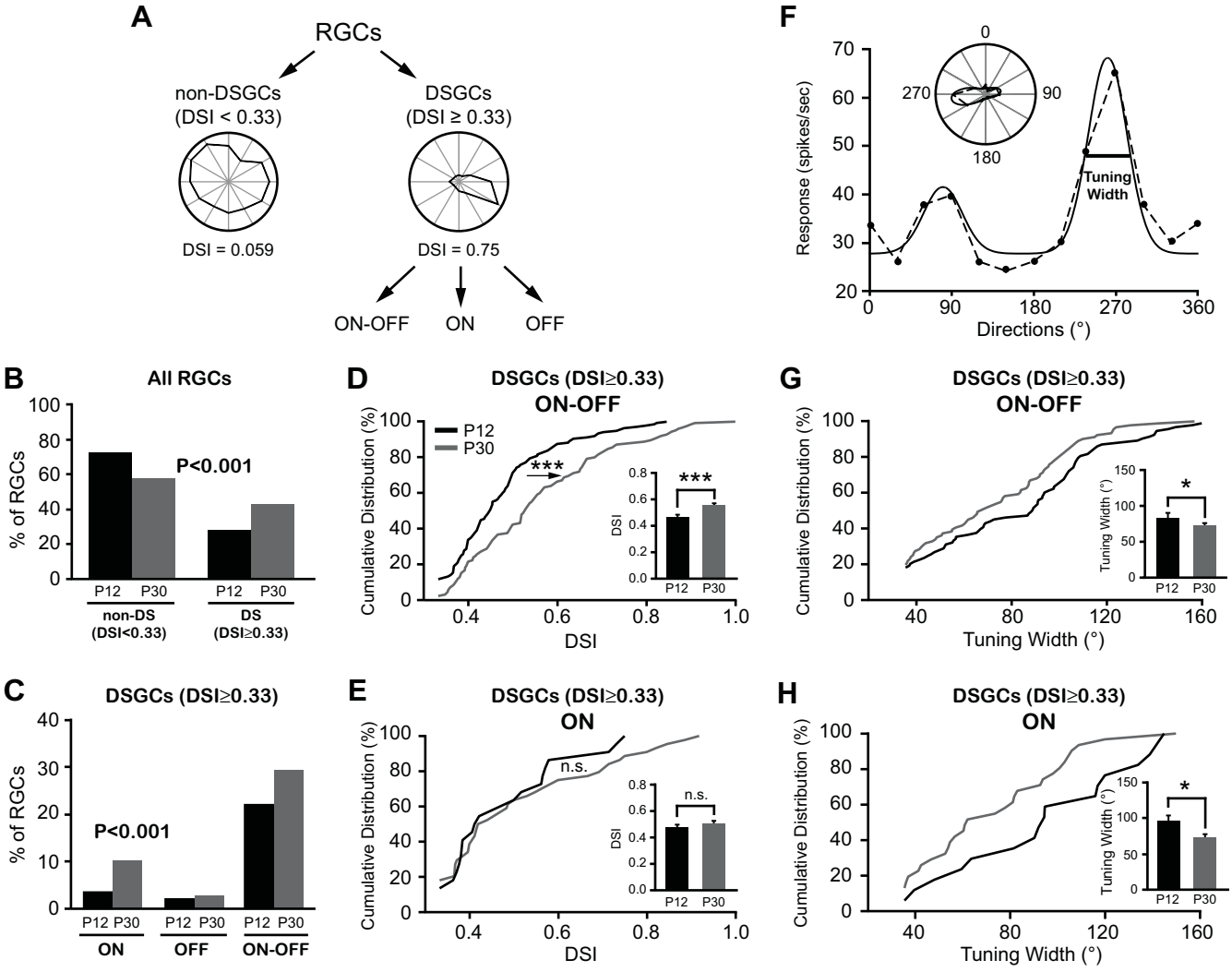
A
RGCs
non-DSGCs
(DSI < 0.33)
DSGCs
(DSI ≥ 0.33)
DSI = 0.059
DSI = 0.75
ON-OFF
ON
OFF
F
Response (spikes/sec)
Directions (°)
Tuning Width
0
90
180
270
B
All RGCs
% of RGCs
P<0.001
P12 P30
non-DS (DSI<0.33)
DS (DSI≥0.33)
C
DSGCs (DSI≥0.33)
% of RGCs
P<0.001
ON
OFF
ON-OFF
D
DSGCs (DSI≥0.33)
ON-OFF
Cumulative Distribution (%)
P12
P30
***
DSI
E
DSGCs (DSI≥0.33)
ON
n.s.
G
DSGCs (DSI≥0.33)
ON-OFF
Tuning Width (°)
*
H
DSGCs (DSI≥0.33)
ON

Figure 4

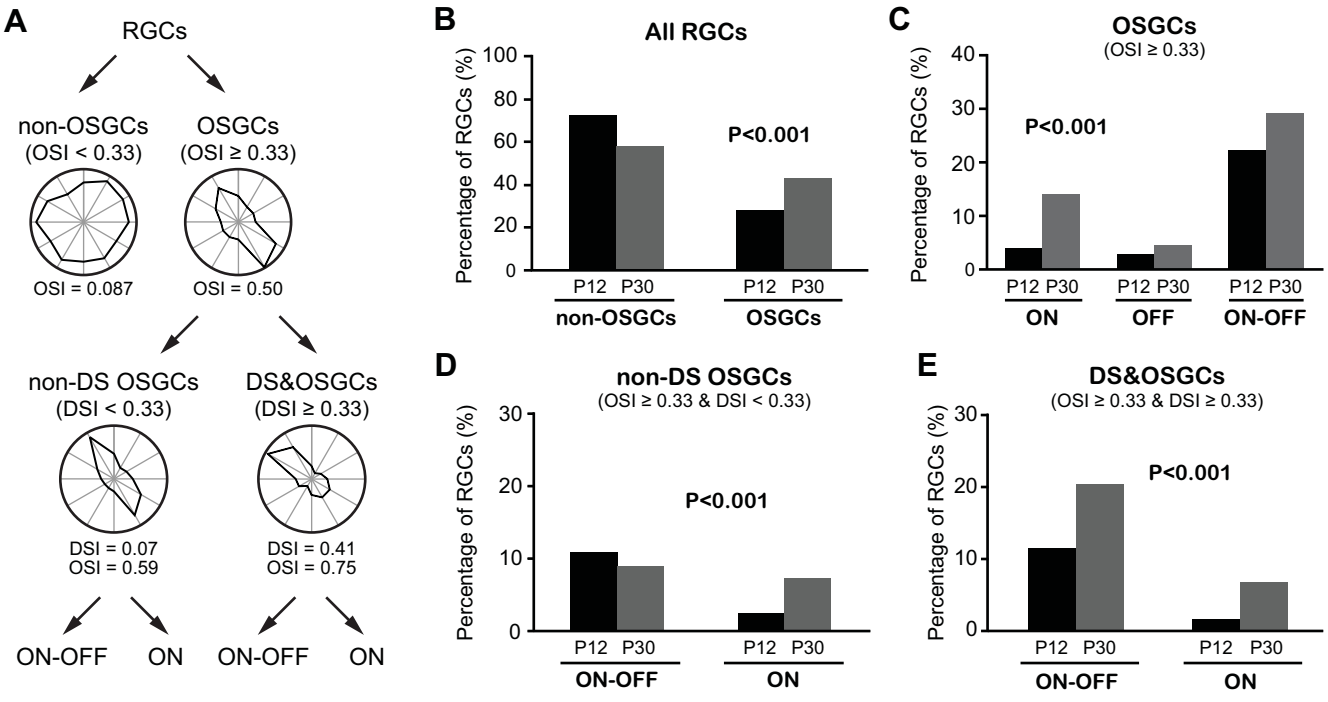
A
RGCs
non-OSGCs
(OSI < 0.33)
OSGCs
(OSI ≥ 0.33)
OSI = 0.087
OSI = 0.50
non-DS OSGCs
(DSI < 0.33)
DS&OSGCs
(DSI ≥ 0.33)
DSI = 0.07
OSI = 0.59
DSI = 0.41
OSI = 0.75
ON-OFF
ON
ON-OFF
ON
B
All RGCs
Percentage of RGCs (%)
P<0.001
P12 P30
P12 P30
non-OSGCs
OSGCs
C
OSGCs
(OSI ≥ 0.33)
Percentage of RGCs (%)
P<0.001
P12 P30
P12 P30
P12 P30
ON
OFF
ON-OFF
D
non-DS OSGCs
(OSI ≥ 0.33 & DSI < 0.33)
Percentage of RGCs (%)
P<0.001
P12 P30
P12 P30
ON-OFF
ON
E
DS&OSGCs
(OSI ≥ 0.33 & DSI ≥ 0.33)
Percentage of RGCs (%)
P<0.001
P12 P30
P12 P30
ON-OFF
ON

Figure 5

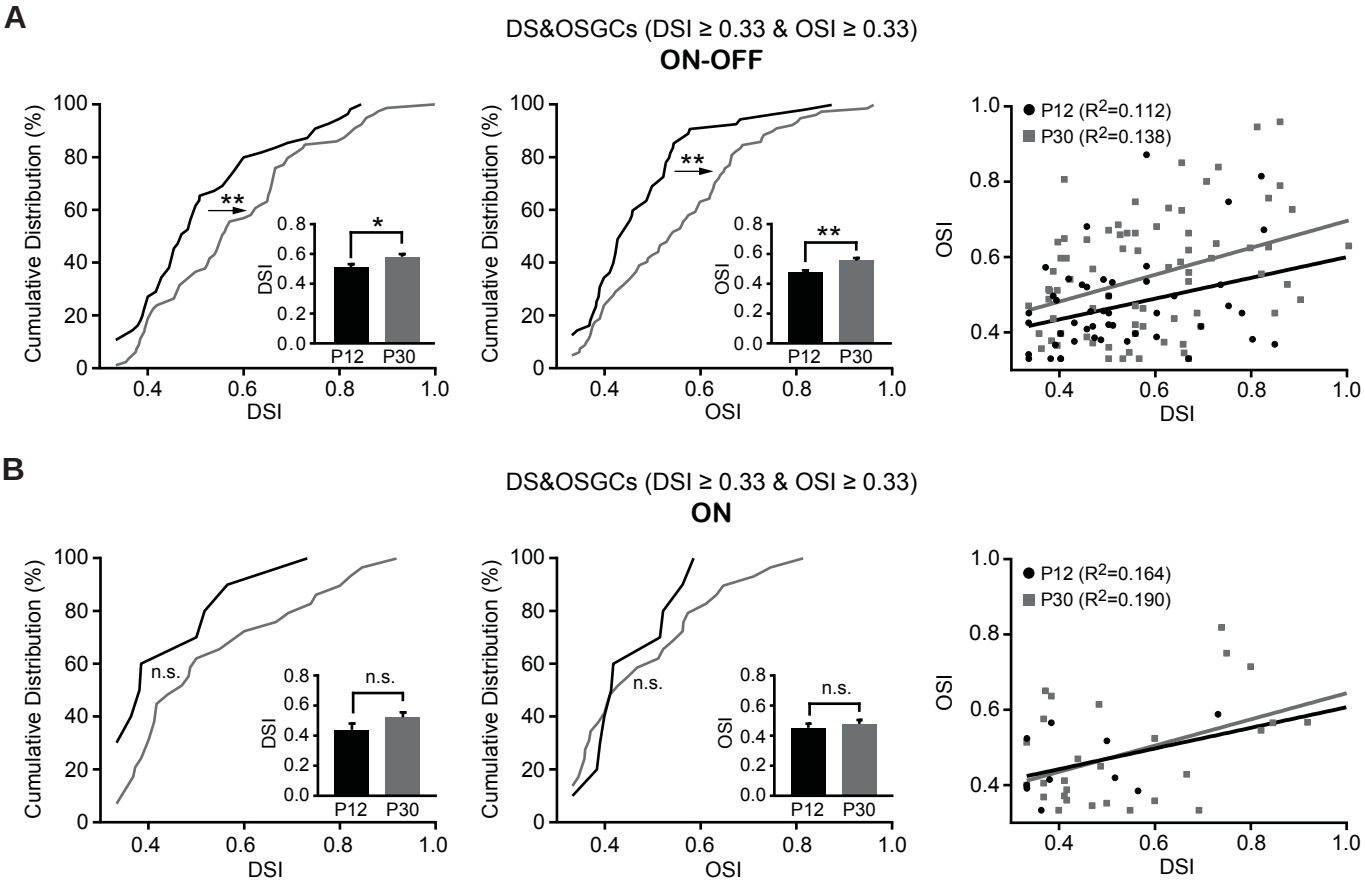
A
DS&OSGCs (DSI ≥ 0.33 & OSI ≥ 0.33)
ON-OFF
Cumulative Distribution (%)
DSI
OSI
P12 (R2=0.112)
P30 (R2=0.138)
B
DS&OSGCs (DSI ≥ 0.33 & OSI ≥ 0.33)
ON
P12 (R2=0.164)
P30 (R2=0.190)
n.s.
P12
P30

Figure 6

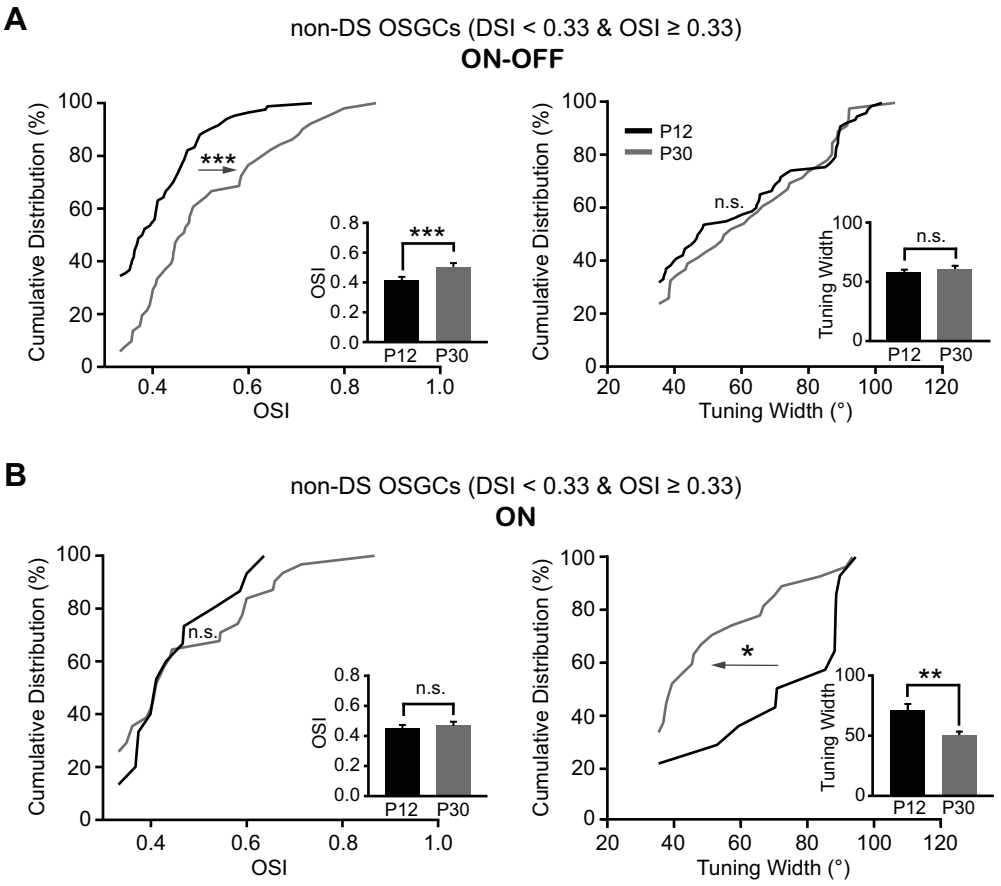
A
non-DS OSGCs (DSI < 0.33 & OSI ≥ 0.33)
ON-OFF
Cumulative Distribution (%)
OSI
***
***
P12
P30
Tuning Width (°)
n.s.
n.s.
Tuning Width
B
non-DS OSGCs (DSI < 0.33 & OSI ≥ 0.33)
ON
n.s.
n.s.
*
**

Table 1. Summary of the numbers of RGCs at P12 and P30

	Number of Retinas	Number of Cells	All RGCs			DSGCs (DSI≥0.33)				OSGCs (OSI≥0.33)			
			ON	OFF	ON-OFF	Total	ON	OFF	ON-OFF	Total	ON	OFF	ON-OFF
P12	4	615	120	67	428	171	22	13	136	180	25	18	137
			19.5%	10.9%	69.6%	27.8%	3.6%	2.1%	22.1%	29.3%	4.1%	2.9%	22.3%
P30	4	425	175	47	203	181	44	12	125	203	60	19	124
			41.2%	11.0%	47.8%	42.6%	10.4%	2.8%	29.4%	47.8%	14.1%	4.5%	29.2%